AD-A031 836 NAVAL RESEARCH LAB WASHINGTON D C F/G 21/5
FATIGUE-CRACK-GROWTH ANALYSIS OF TITANIUM GAS-TURBINE FAN BLADE--ETC(U)
OCT 76 W H CULLEN, F R STONESIFER

UNCLASSIFIED NRL-MR-3378 NL

| OF |
AD
A031 836

END

DATE
FILMED
12-76

NRL Memorandum Report 3378

Fatigue-Crack-Growth Analysis of Titanium Gas-Turbine Fan Blades

W. H. CULLEN AND F. R. STONESIFER

Mechanics of Materials Branch
Ocean Technology Division

October 1976

NAVAL RESEARCH LABORATORY
Washington, D.C.

SECURITY CLASSIFICATION OF THIS PAGE (When Data Entered)

REPORT DOCUMENTATION PAGE

READ INSTRUCTIONS BEFORE COMPLETING FORM

1. REPORT NUMBER: NRL Memorandum Report 3378
2. GOVT ACCESSION NO.
3. RECIPIENT'S CATALOG NUMBER

4. TITLE (and Subtitle): FATIGUE-CRACK-GROWTH ANALYSIS OF TITANIUM GAS-TURBINE FAN BLADES

5. TYPE OF REPORT & PERIOD COVERED: Interim report on a continuing NRL problem.
6. PERFORMING ORG. REPORT NUMBER

7. AUTHOR(s): W. H. Cullen and F. R. Stonesifer
8. CONTRACT OR GRANT NUMBER(s)

9. PERFORMING ORGANIZATION NAME AND ADDRESS: Naval Research Laboratory, Washington, D.C. 20375
10. PROGRAM ELEMENT, PROJECT, TASK AREA & WORK UNIT NUMBERS: NRL Problem F01-24, Project WR-022-01-001

11. CONTROLLING OFFICE NAME AND ADDRESS: Naval Air Systems Command, Aerodynamic Materials and Structures Section, Washington, D.C. 20360
12. REPORT DATE: October 1976
13. NUMBER OF PAGES: 30

14. MONITORING AGENCY NAME & ADDRESS (if different from Controlling Office)
15. SECURITY CLASS. (of this report): UNCLASSIFIED
15a. DECLASSIFICATION/DOWNGRADING SCHEDULE

16. DISTRIBUTION STATEMENT (of this Report)

Approved for public release; distribution unlimited.

NRL-MR-3378

17. DISTRIBUTION STATEMENT (of the abstract entered in Block 20, if different from Report)

18. SUPPLEMENTARY NOTES

19. KEY WORDS (Continue on reverse side if necessary and identify by block number)

Titanium alloys
Ti-8Al-1Mo-1V
Corrosion fatigue
Gas turbine engines
Stress analysis

20. ABSTRACT (Continue on reverse side if necessary and identify by block number)

First stage forged titanium gas turbine fan blades from a military aircraft were removed from service, cut into specimens and tested for fatigue crack growth properties. A method for determining stress intensity based on change in compliance with increasing crack length was applied. Results of testing in air and salt water environments are presented. A model, based on stress-strain curve behavior, is developed and applied to simulate the data. The data is compared to that taken from rolled baseplate forms of the same material and the applicability of the data to fan blade design and lifetime estimates is discussed.

DD FORM 1 JAN 73 1473 EDITION OF 1 NOV 65 IS OBSOLETE
S/N 0102-014-6601

SECURITY CLASSIFICATION OF THIS PAGE (When Data Entered)

251 950 LB

CONTENTS

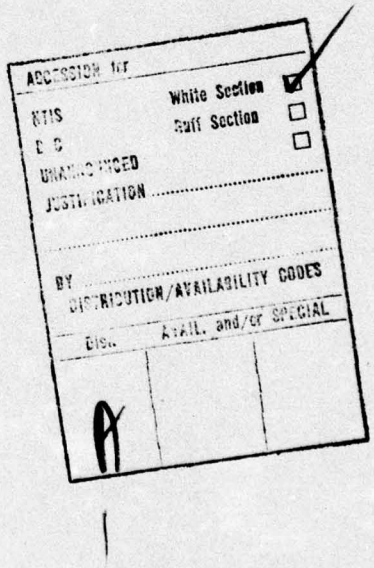

FATIGUE-CRACK-GROWTH ANALYSIS OF TITANIUM GAS-TURBINE FAN BLADES

INTRODUCTION

The use of titanium alloys for both rotating and static components in the near-ambient temperature sections of gas-turbine engines became a well-established practice in the 1960's. Both commercial and military aircraft engines contain forged titanium fan blades and disks or hubs in their primary stages. The use of titanium follows naturally from the moderately high strength and low weight of these materials. As additional credits, these materials are creep resistant, and have good fracture and crack growth resistance. Within the framework of titanium alloys, Ti-8Al-1Mo-1V was singled out for use because of its slightly higher Young's Modulus, E, 113-124 GPa (16,500-18,000 ksi) and slightly lower density, ρ, 4.37-4.43 x 10^3 kg/m^3 (0.158-0.160 lbs/in^3). Since the vibrational frequencies for a blade of fixed geometry are proportional to $\sqrt{E/\rho}$, the choice of Ti-8-1-1 raises these resonant frequencies (and their harmonics) by about 7% over other possible choices of Ti-base materials, and thus allows correspondingly higher engine speeds.

However, research on the Ti-8-1-1 material in rolled baseplate form has revealed that it is sensitive to environmentally assisted crack growth. Several research efforts at the Naval Research Laboratory in the fields of stress-corrosion cracking [1,2] and corrosion fatigue [3] supplemented by research elsewhere [4,5] combine to demonstrate the aggressive, detrimental effect of salt solutions on the

1. B. F. Brown, "A New Stress-Corrosion Cracking Test for High Strength Alloys," Materials Research and Standards, 66, (3), pp. 129-133, March 1966.
2. A. M. Sullivan, "Velocity of Cracks Extending Under Stress in an Adverse Environment", Fracture, Proc. 2nd Int. Conf. on Fracture, Chapman-Hall, Ltd. pp. 396-405, (1969).
3. D. A. Meyn, "An Analysis of Frequency and Amplitude Effects on Corrosion Fatigue Crack Propagation in Ti-8Al-1Mo-1V," Met. Trans. 2, pp. 853-865, March 1971.
4. R. J. Bucci and P. C. Paris, "Fatigue Behavior of a Titanium 8Al-1Mo-1V Alloy in a Dry Argon Environment," Journal of Materials 7(3), pp. 402-409, September 1972.
5. R. J. H. Wanhill, "A Review and Analysis of Fatigue Crack Propagation in Titanium Alloys at Room Temperature," National Aerospace Laboratory Report #NLR-TR-71035U 1971.

Manuscript submitted September 10, 1976.

subcritical crack growth rates. Variations in stage II fatigue-crack-growth rates per cycle (at some explicit value of applied stress intensity) of over two orders of magnitude can be achieved by certain judicious (or unfortunate) choices of loading frequencies and environments.

Thus, it is clear that operation of gas-turbine engines in salt-water/salt-air environments could lead to stress-corrosion cracking problems. More recently, the Navy is considering the use of the gas-turbine engine as the prime mover for the Spruance destroyer class. The initial development approach is to "marinize" some existing form of an aircraft power plant. However, since the atmosphere near the air-sea interface is laden with particles of both continental and oceanic origins, [6], the environmental degradation of these marine gas turbines has become a question of immediate concern.

Occasional failures in a certain class of engine have been brought to the attention of NRL personnel and a project to determine the sensitivity of environmentally-assisted cracking of the as-fabricated forged titanium first stage fan blade was begun. In practice, it was found that the forging process often left glass-lubricant-filled laps along the edges of the blade, and either these, or foreign object damage, provided the nucleus of a subcritical crack. With the problem thus removed from the realm of fatigue crack nucleation, and the lifetime estimates thus determined by fatigue crack propagation, the knowledge of fatigue crack growth rates becomes an engineering design factor. The problem reduces to the question, (given the initial flaw) what are the fatigue crack growth rate characteristics?

There were two objectives in this study. The first was to develop an experimental procedure for determining the stress-intensity factor for cracks in production turbine blades. The non-uniform thickness and foil shape of the blades necessitate calculation of the stress intensity factor from the change in the specimen compliance with respect to crack length. The second objective was to determine crack growth rates, at ambient temperature, in both room air and 3.5% salt solution. These two conditions should represent the environmental extremes to which these turbines are subjected.

---

6. W. H. Cullen, P. E. Wilkness, D. J. Bressan, "Analysis of Marine Aerosols by Combined Scanning Electron Microscopy and Energy Dispersive Analysis," NRL Memorandum Report #3017, March 1975.

SPECIMEN CONSIDERATIONS

The Naval Research Laboratory was furnished with several first-stage fan blades which had been removed from service because of foreign object damage. The processing of these blades had been accomplished in a series of steps. From initial stock, the root and span were upset at about 1250K (1800°F), cooled and cleaned, followed by preforming at the same temperature, cooling and cleaning. The blades were solution treated at 1170-1200 ±12K (1650-1700°F ± 25°F) for one hour and air cooled. Any dimension correction required was then performed and the blades were aged at 480-870K (1050-1100°F) for eight hours and air cooled. The root was machined to its final dimension and the foil was sanded. The final operation was a stress relief at 810K (1000°F) for two hours followed by air cooling. This thermomechanical routine results in the microstructure shown in Figure 1.

Compact fracture specimens (Fig. 2) were cut from each blade from locations at either side of the midspan shroud. These were oriented as in Figure 3 such that the crack propagated from the leading edge toward the trailing edge when the load was applied parallel to the longitudinal axis of the blade. This corresponded to the suspected in-service failure path and primary stress. A single-edge-notch tension type of specimen appears to be the only acceptable geometry for a fracture mechanics type of analysis. The variable, unsymmetrical change in thickness across the width of the blade disqualifies use of a part-through crack or center cracked panel type of specimen, and the extreme thinness will not allow the use of any type of bending specimen.

Locating the compact-fracture specimens on either side of the midspan shroud created specimens which fell into two geometrical classes, characterized primarily by the different thickness of specimens from either of the two locations. However specimens within the same class had similar thickness gradients from front-to-back and side-to-side, and nearly the same warp, which amounted to about 15° of twist per specimen. The classification of specimens in this way will be employed in the following sections to expedite the experimental analysis of the blades.

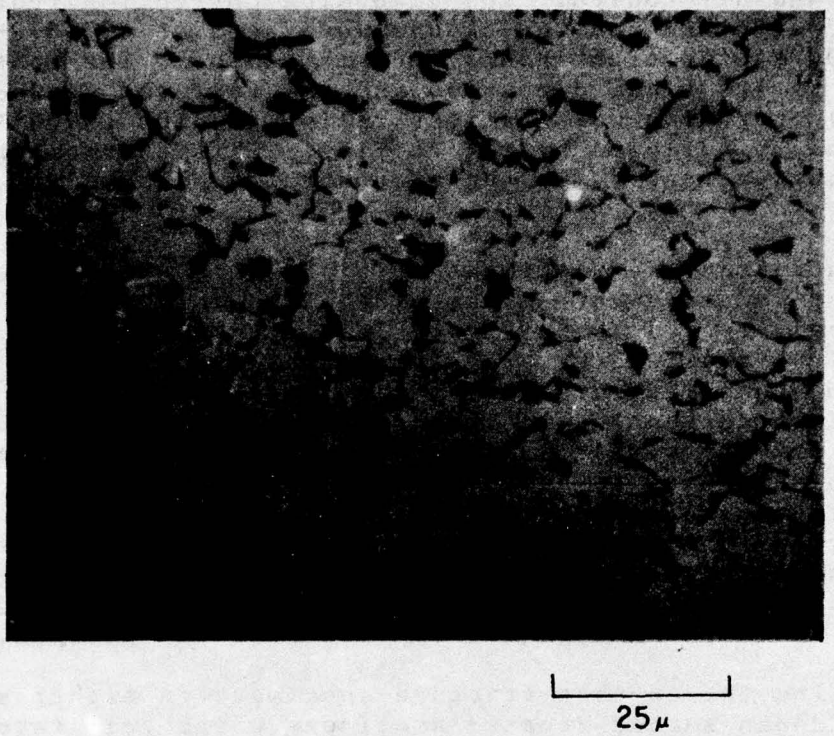

Fig. 1 — The microstructure of the forged fan blades in the plane parallel to the fatigue fracture surface. The microstructure is relatively equiaxed alpha phase (white) mixed with intergranular beta (dark).

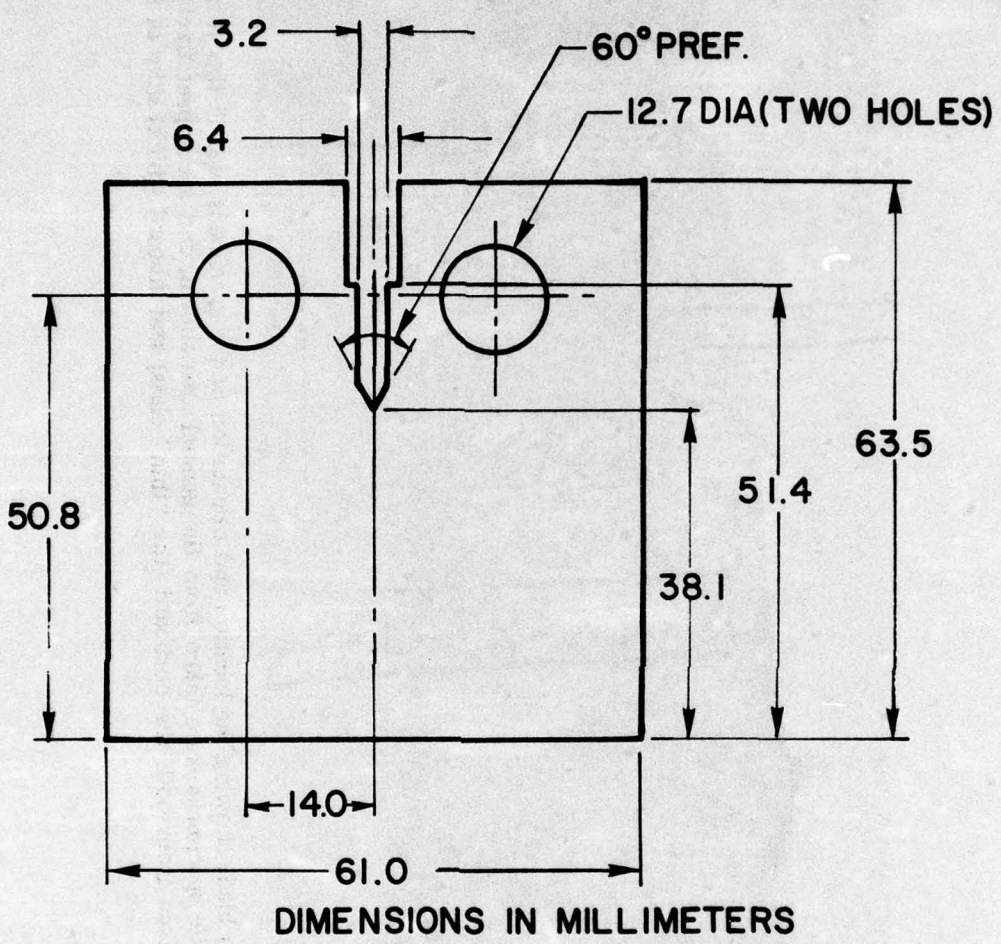

Fig. 2 — The fracture specimen used in this study. Based on the customary ASTM compact fracture specimen, this piece has an enlarged notch so that a clip gage may be inserted and the displacement along the load line recorded. The bearing surfaces of the clip gage extended 0.6 mm into the narrow notch and were directly on the load line. All dimensions in millimeters.

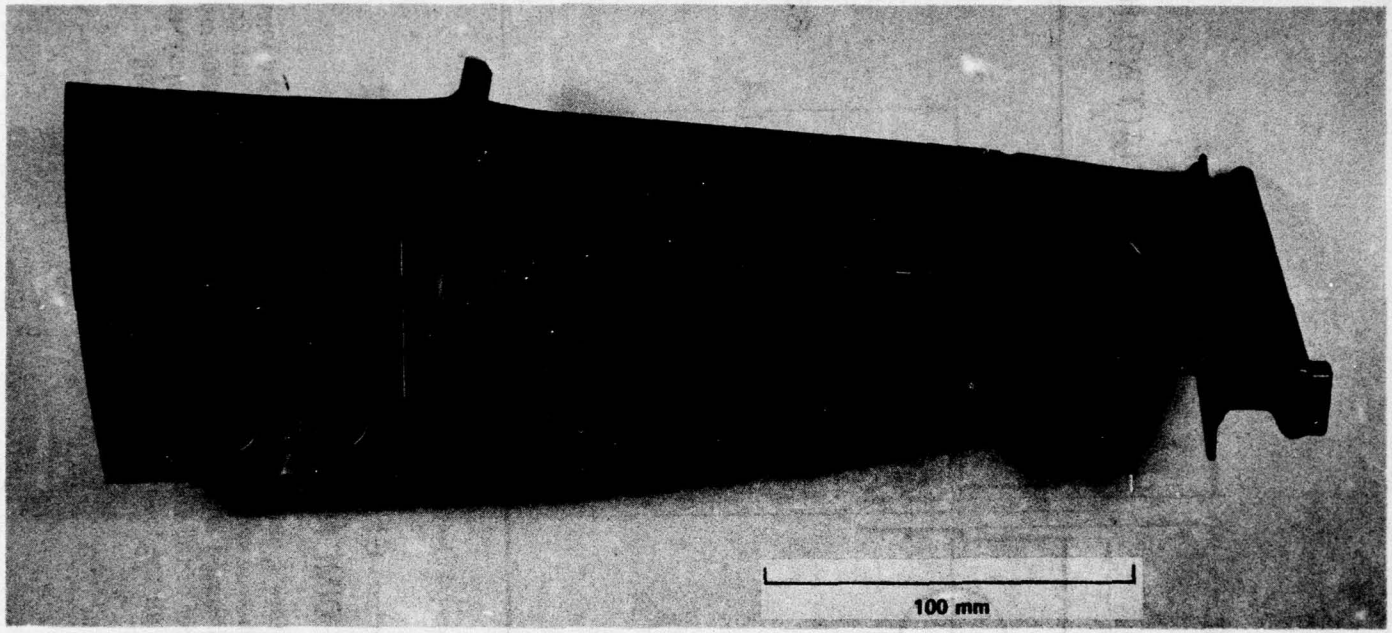

Fig. 3 — The fan blade showing the location and orientation of the specimens used in this study. Up to four tensile specimens were taken from the general area shown, and a compact fracture specimen was taken from both the outboard (the "thin" class) and inboard (thick) sides of the shroud fin.

METHOD OF ANALYSIS

The method for calculating the stress intensity at the tip of a subcritical crack in these blades is based on the calculation of the stress field energy loss per unit crack extension due to Irwin [7]. This treatment is more explicitly presented by Kies, Smith, Romine and Bernstein [8]. Essentially, this stress field energy loss, $\mathcal{G}$, (also called strain energy release rate) is given by

$$\mathcal{G} = \frac{P^2}{2} \frac{d(1/M)}{dA}$$

where P is the load on the specimen, A is the cracked area created by the load, and the spring constant, 1/M, is related to the elastic deflection, δ, by

$$\delta = P/M$$

It is essential that the deflection δ either be measured along the load line or if measured elsewhere, be geometrically referred to the load line, so that the proper numeric value of $\mathcal{G}$ will be obtained. Since, for straight crack fronts dA = Bda, where B is the specimen thickness and a is the crack length

$$\mathcal{G} = \frac{P^2}{2B} \frac{d(1/M)}{da} \tag{1}$$

and by definition, the stress intensity

$$K_2 = \frac{E\mathcal{G}}{1-\nu^2} \tag{2}$$

in which E is Young's modulus for the material, and ν is the Poisson ratio. The term $1-\nu^2$ is included for a plane strain fracture behavior, but deleted for plane stress situations.

---

7. G. R. Irwin, "Fracture Testing of High-Strength Sheet Materials Under Conditions Appropriate for Stress Analysis," NRL Report #5486, July 1960.

8. J. R. Kies, H. L. Smith, H. E. Romine and H. Bernstein, "Fracture Testing of Weldments," in Fracture Toughness Testing and Its Applications, ASTM-STP#381, American Society for Testing and Materials, Philadelphia, Pennsylvania 19103.

EXPERIMENTAL METHOD

Compact type fracture specimens, with full blade thickness, were tested using a closed loop system operating in the load-control mode. The load-time profile was a sine wave with the R ratio (min load/max load) maintained at 0.1. Samples tested in air were cycled at 5.0 Hz while those in salt water environment were cycled at 0.5Hz. The output from an ASTM (E399) [9] type clip gage was plotted against that of the load cell using an X - Y recorder to produce a permanent record. Specimen compliance could then easily be determined from this record. The specimens were machined so that the clip gage pivoted on the load line. Sullivan [10] found that although different absolute values are obtained for the displacement, or crack opening, measured on the load line as opposed to that measured at the specimen ends and referred to the load line, the slopes or derivatives of the two data sets are nearly identical.

Tests were performed in two different environments, both at ambient room temperature. As base line data, specimens were tested in normal laboratory air for comparison with salt water results. These latter data were obtained from specimens with an absorbent strip of cloth pulled loosely into the machined notch and knotted at the back edge. This cloth was kept soaked with a 3.5% solution of NaCl in distilled H_2O.

The first seven specimens (four in air and three in salt water) were removed from the testing grips after each compliance measurement so that the crack length could be visually measured on both surfaces of the specimen with a traveling microscope. Although the specimen surfaces had been polished, it was still difficult to visually locate the crack tip when the specimen was unloaded. This difficulty caused some small local irregularities on the plot of displacement/load versus crack length.

---

9. Standard Method of Test for Plane-Strain Fracture Toughness of Metallic Materials, Designation E399-72, in 1973 Annual Book of ASTM Standards, American Society for Testing and Materials, Philadelphia, Pa.19103.

10. A. M. Sullivan, "Crack Length Determination for the Compact Tension Specimen Using a Crack-Opening-Displacement Calibration," NRL Report 7888, June 1975.

Smooth curves were drawn by hand so as to best fit the data for both the thick and thin specimens. It was found that the curves were identical except displaced along the ordinate axis by 5.714 nm/N(1 x 10^{-6} in./lb). The environment, of course, had no effect on the calibration. Evenly spaced values were read from this master calibration curve and used to generate a computer fitted polynomial representation of the displacement/load vs crack length. The resulting equation, for the thin specimens is

$$\frac{\delta}{P} = k_o + k_1\left(\frac{a}{W}\right) + k_2\left(\frac{a}{W}\right)^2 + k_3\left(\frac{a}{W}\right)^3 + k_4\left(\frac{a}{W}\right)^4 \qquad (3)$$

in which

$k_o = 0.30776$ μm/N

$k_1 = -3.0012$

$k_2 = 11.5887$

$k_3 = -19.1922$

$k_4 = 12.3084$

For thick specimens, the constant term becomes $k_o' = k_o - 5.714$ nm/N = 0.30205 μm/N. Differentiating Eq. (3) yields the slope of the displacement/load vs crack length curve which is necessary for the calculation of G, as in Eq. (1).

$$d(\delta/P)/da = \frac{1}{W}\left[j_o + j_1\left(\frac{a}{W}\right) + j_2\left(\frac{a}{W}\right)^2 + j_3\left(\frac{a}{W}\right)^3\right] \qquad (4)$$

in which $j_o = k_1 = -3.0012$ μm/N

$j_1 = 2k_2 = 23.1774$

$j_2 = 3k_3 = -57.5766$

$j_3 = 4k_4 = 49.2336$

Since the displacement/load could be measured more accurately and easily than the visual crack length, this was used as the measured experimental parameter, with the corresponding crack length being read from the calibration curve. The appropriate $\frac{\delta c}{\delta a}$ was then read from a graph of Eq. (4)

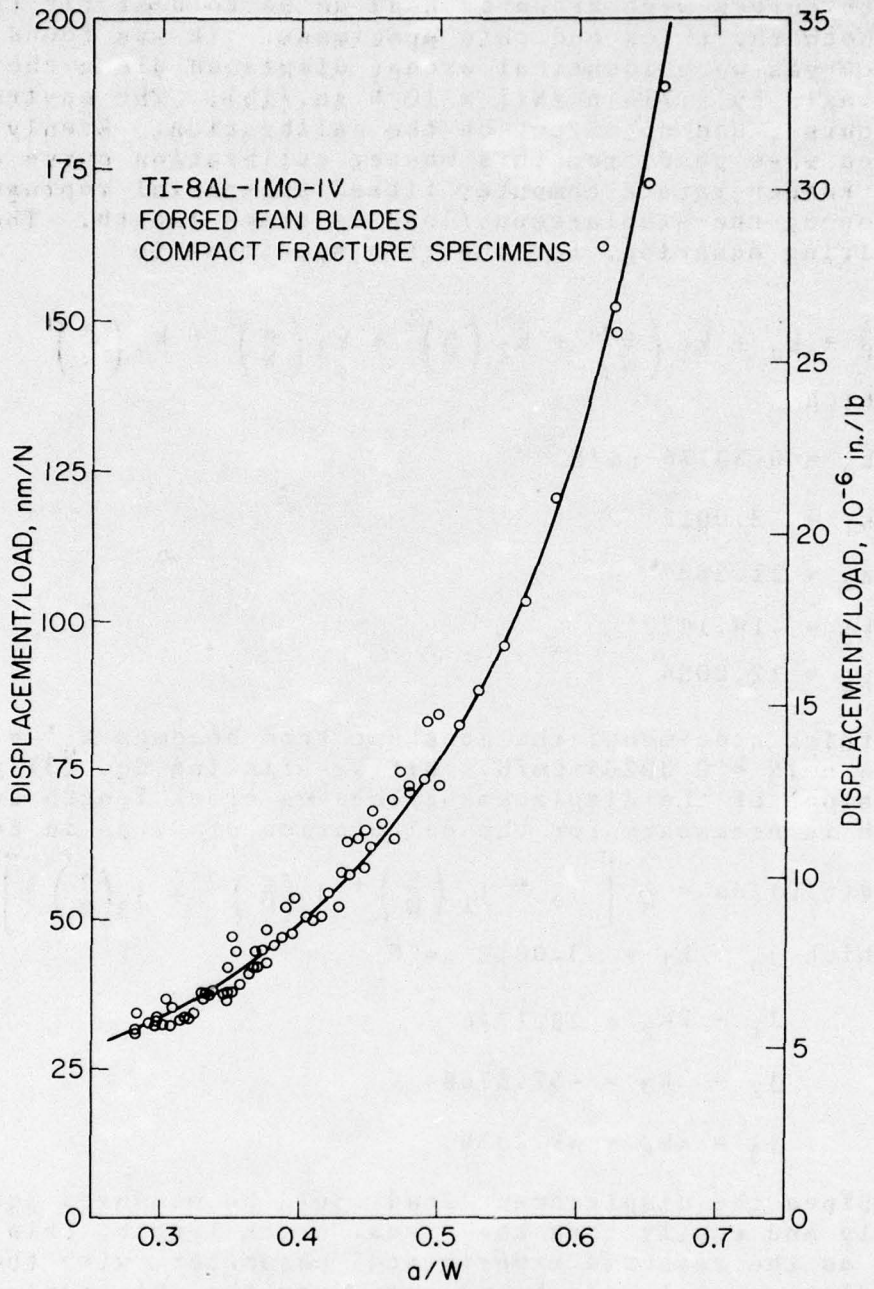

Fig. 4 — The displacement/load vs normalized crack length for the thin class of specimens. The curve was hand-drawn through the data and an expression (Eq. (3)) was derived for points taken from the curve.

for the same value of crack length as determined from the first curve. The data used in defining the calibration curves was then reused along with additional data for plotting the crack growth rate vs applied stress intensity curves. So for all specimens, the measured compliance was used to graphically determine crack length. These values were then used in the final calculation rather than the visual crack measurements. Since the master curves were now well established, only the compliance needed to be measured for the remaining test specimens.

The specimen thickness was measured with a micrometer at 2.5 mm intervals along the expected path of the propagating crack. These measurements were magnified by a factor of 10 and plotted on graph paper. A smooth curve through these points gave a 10X profile of the specimen thickness, which could then be accurately determined at any point on the crack line. The thickness at each data-point value of crack length was read from the profile plot and used in the ΔK calculations. Values of ΔK were calculated using Eqs. (1) and (2) above, and plotted against da/dN values on log-log paper in the normal manner. The da/dN values were obtained by simply dividing the increase in crack length, Δa, by the number of load cycles, ΔN, applied to the specimen during the crack growth interval.

There was some difficulty in keeping the crack propagating toward the back edge along a line parallel to the machined notch as illustrated in Fig. 5. This problem occurred to some degree in 6 of 8 salt water tests and 2 of 4 room air tests. Since the specimens had a slight thickness variation in the direction perpendicular to the machined notch, once the crack curved toward the thinner side it was virtually impossible to straighten it. Reinitiating the crack from a new more deeply machined notch was impractical. The notch had to be so deep, to compensate for the natural crack tip sharpness and reduced specimen thickness, as to render the remaining specimen section too small to be of any value for further crack propagation measurements. Only that data gathered while the crack was reasonably straight could be used with confidence.

As data input for the tensile ligament model calculations, stress-strain and stress relaxation values for this material were needed. For this purpose, subsize tension-compression (4 mm gage diameter x 11 mm gage length) were fabricated from near the root of the fan blade at the approximate location shown in Fig. 3. The axis of these specimens was parallel to the longitudinal axis of the fan blade and hence normal to the fracture plane of the compact fracture specimen.

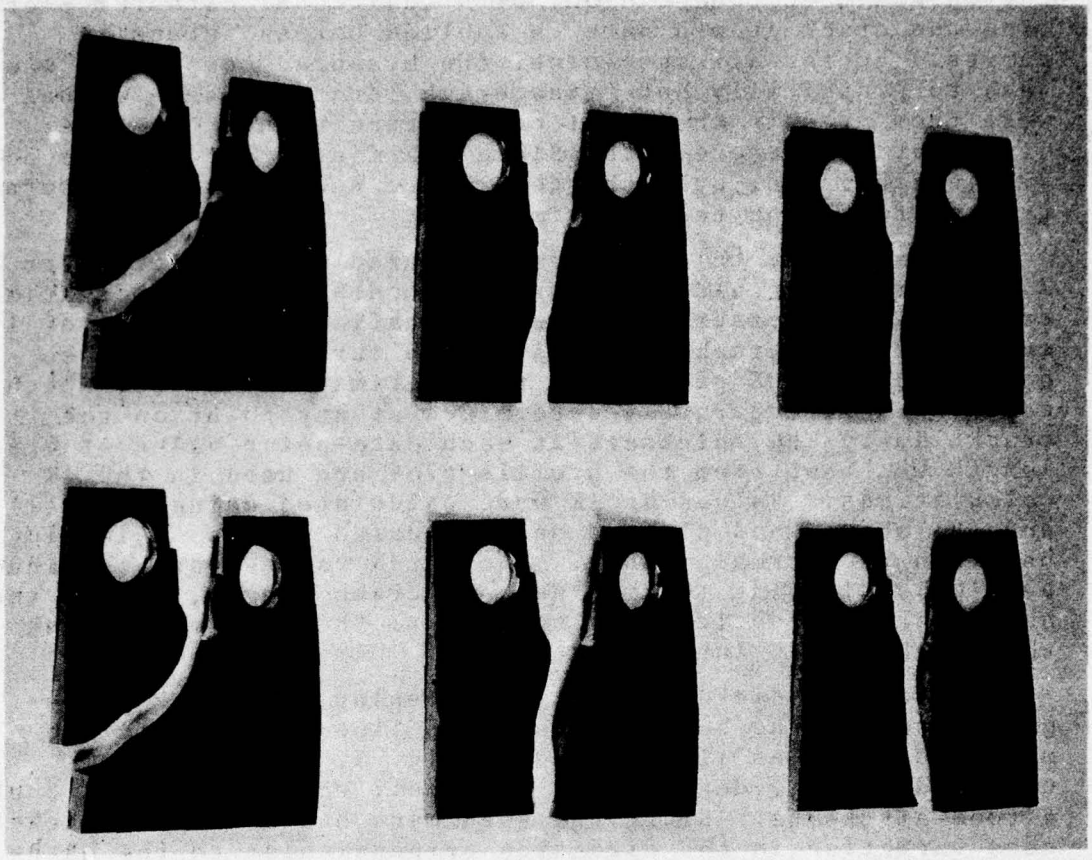

Fig. 5 — Examples of the fatigue fractured samples. The path of the crack bore no relationship to specimen thickness or the combinations of frequency and environment used.

Complete details of the experimental stress-strain procedure can be found elsewhere [11]. The pertinent results of over twenty tests on seven fan blades are contained in Table 1. For the purpose of modeling, the uniaxial stress-diametral strain data must be converted to true stress-natural linear strain. The following formulas were used to accomplish this: (ℓ - linear, d - diametral, p - plastic, e_i - engineering strain, $\bar{\varepsilon}_i$ - natural strain, i = 1, first excursion or 2, second excursion)

$$\bar{\varepsilon}_{id} = -\log_e (1 - e_{id})$$

$$\bar{\varepsilon}_{idp} = \bar{\varepsilon}_{id} - \sigma_i/\theta_o$$

$$\bar{\varepsilon}_{i1p} = -2\bar{\varepsilon}_{idp}$$

$$= -2\left[-\log_e (1-e_{id}) - \bar{\sigma}_i/\theta_o\right] \qquad (5)$$

$$\bar{\varepsilon}_{i1} = \bar{\varepsilon}_{i1p} + \bar{\sigma}_i/E$$

In these equations, θ_o is the elastic modulus for diametral strain, ($E \simeq \nu\theta_o$)).

From this point on, the letter ℓ is dropped from the strain subscripting and all strains are assumed to be linear.

The recorded engineering stress-diametral strain curves were converted to true stress-natural linear strain at about twenty points spanning the range from 0.05% plastic strain to just beyond instability for both first and second excursion records. A constitutive equation of a form due to Gladman, Holmes and Pickering [12],

$$\bar{\sigma}_2 = A + B \log_e (\bar{\varepsilon}_{2p}) + C(\bar{\varepsilon}_{2p}), \qquad (6)$$

---

11. J. M. Krafft, "Method for Relating Plastic Flow Properties to Fatigue Crack Propagation Including Effects of Stress Ratio," NRL Memorandum Report #2980, January 1975.

12. T. Gladmon, B. Holmes and F. B. Pickering, "Work Hardening of Low-Carbon Steels," J. Iron and Steel Inst., pp. 172-183, 1970.

TABLE I. Results of tensile tests of specimens taken from seven different first stage fan blades: σ_{pl} - proportional limit stress; σ_{ys} - yield stress at 0.2% strain offset; $\sigma_{uts,1}$, $\varepsilon_{uts,1}$ - ultimate stress and strain during first excursion; σ_{ucs} - compressive stress needed to return specimen to zero strain, $\sigma_{uts,2}$, $\varepsilon_{uts,2}$ - ultimate stress and strain during second excursion. All stresses in kilopascals.

Test #	σ_{pl}	σ_{ys}	$\sigma_{uts,1}$	$\varepsilon_{uts,1}$	σ_{ucs}	$\sigma_{uts,2}$	$\varepsilon_{uts,2}$
7215	965	1058	1158	$.12_0$	-1407	1198	$.05_4$
7216	730	931	1027	$.05_0$	-1151	1127	$.06_4$
7244	870	1042	1125	$.12_5$	-1351	1143	$.08_2$
7245	980	1065	1132	$.11_0$	-1358	1146	$.07_1$
7246	910	1025	1118	$.11_0$	-1365	1143	$.07_7$
7247	870	998	1127	$.11_5$	-1241	1124	$.06_6$
7247A	855	1008	1127	$.14_0$	-1317	1155	$.07_1$
7247B	815	1022	1096	$.11_0$	-1358	1122	$.06_6$
7252	880	994	1086	$.09_5$	-1317	1091	$.05_6$
7253	965	1024	1089	$.13_5$	-1393	1122	$.06_1$
7254	965	1041	1110	$.11_4$	-1351	1122	$.06_3$
7255	950	1038	1103	$.13_5$	-1407	1143	$.08_1$
7256	870	1014	1117	$.11_5$	-1386	1117	$.07_0$
7257	815	910	1048	$.12_5$	-1358	1073	$.09_0$
7258	595	800	962	$.07_8$	-1165	943	$.05_1$
7259	815	948	997	$.06_5$	-1241	1012	$.07_2$
7260	910	1058	1117	$.11_0$	-1365	1131	$.07_2$
7261	925	1058	1162	$.14_0$	-1434	1196	$.07_9$
7262	885	1031	1138	$.12_5$	-1420	1162	$.07_0$
7263	840	976	1091	$.10_5$	-1351	1109	$.07_0$

was fit to the second cycle data. A generalized Newton-Raphson method was used to find A, B, and C. This equation can be differentiated to find the plastic work-hardening coefficient,

$$\Theta_{2p} = d\bar{\sigma}_2/d\bar{\epsilon}_{2p}.$$

An attempt was made to fit the first excursion true stress-natural plastic strain data to a Hollomon-type equation [13]

$$\bar{\sigma}_1 = C(\bar{\epsilon}_{1p})^n,$$

in which n is taken to be the strain-hardening exponent. However, the two stage work-hardening behavior of this material precludes the representation of the stress-strain curve by one such equation. Thus, as a more practical, but less flexible method, values taken directly from the engineering stress-strain curve may be substituted directly into the formulas, with the modification that

$$\frac{\Theta_1}{\sigma_1} - Z = \frac{\Theta_{1T}}{\sigma_{1T}} + (1-Z).$$

Thus, in the figures of the following section, modeling curves based on second cycle data are smooth and continuous, whereas curves based on first excursion data are broken, but are made continuous by joining individually calculated points.

MODELING METHODS

The phenomenological description of the tensile ligament instability model, and the derivation of the equations relating plastic flow properties to stress intensities and crack growth rates are presented in complete form in Ref. [14]. The resultant formulas for fatigue crack growth representation using second excursion tensile data, of a corrosive environment ($V_s = 0$), are:

---

13. H. J. Kleemola and M. A. Nieminen, "On The Strain Hardening Parameters of Metals," Met. Trans. 5, pp. 1863-1866, 1974.

14. H. L. Smith, C. L. Lamb, W. H. Cullen, "Low-Frequency, Salt-Water Fatigue Crack Growth in Ti-6Al-2Nb-1Ta-0.8Mo Plate," NRL Report #7966, April 1976.

$$\Delta\varepsilon_{K2} = \bar{\varepsilon}_2 + \sigma_{ucs}/E - R\sigma_{ys}/E \tag{7a}$$

$$\varepsilon_{K2} = \Delta\varepsilon_K/(1-R) \tag{7b}$$

$$K = \sqrt{2\pi d_T}\ E\ \varepsilon_{K2} \tag{7c}$$

$$\Delta K = (1-R)K \tag{7d}$$

$$da/dN\Big|_{cyclic} = \left[2md_T \log_e(t_f/t_o)\right] \left[\varepsilon_{K2}\left(\frac{\Theta_{2P}}{\bar{\sigma}_2} - Z\right)\right]^{-1} \tag{7e}$$

in which

σ_{ys}, σ_{ucs} = tensile yield and ultimate compressive stresses

E = Young's modulus

Z = triaxial strain correction factor

m = stress-relaxation coefficient

t_f, t_o = hold time and loading time of the fatigue cycle

d_T = tensile ligament diameter (micron-sized)

We call the term in square brackets the growth rate factor, GRF_2, so that

$$GRF_2 = \left[\Delta\varepsilon_{K2}\left(\frac{\Theta_{2P}}{\bar{\sigma}_2} - Z\right)\right]^{-1} \tag{8}$$

Similarly, the formulas for the stress-corrosion cracking contribution to fatigue crack growth based on first excursion data and using the point-by-point computation method described above are:

$$\varepsilon_{K1} = \bar{\varepsilon}_1 + \left(\frac{1}{1-2\nu} - 1\right)\sigma_{ys}/E \tag{9a}$$

$$\varepsilon_{K1} = \Delta\varepsilon_{K1}/(1-R) \tag{9b}$$

$$da/dN\Big|_{SCC} = 8ZV_s\Delta t \left\{\varepsilon_{K1}\left[\frac{\Theta_1}{\bar{\sigma}_1} + (1-Z)\right]\right\}^{-1} \tag{9c}$$

in which V_s is the corrosion rate of the ligament periphery and $\Delta t = t_f - t_o$. As before, we set

$$GRF_1 = \left\{ \Delta\varepsilon_{K1} \left[\frac{\Theta_1}{\bar{\sigma}_1} + (1-Z) \right] \right\}^{-1} \tag{10}$$

The parameters d_T and V_s are evaluated through the actual matching procedure of the modeling curves to the fatigue crack growth data. A step-by-step procedure for the determination of d_T is shown in Fig. 6. In this step, $da/dN|_{cyclic}$ should be matched to vacuum or inert atmosphere fatigue crack growth data. This would validate the assumption that $V_s = 0$ and Eq. (7e) simplifies to

$$da/dN = 1.2\ m d_T \cdot GRF_2$$

in which $\ln(t_f/t_o) \simeq 0.6$ for a sine wave.

To carry out this procedure, both the data forms (da/dN vs ΔK and GRF_2 vs $\Delta\varepsilon_{K2}$) must be plotted on log-log graph paper of identical scaling. Experience has shown that a good choice for the match point on the GRF_2 ($\Delta\varepsilon_{K2}$) plot is:

$$GRF_2 = 1 \tag{11a}$$

$$\Delta\varepsilon_{K2} = \frac{1000\ MPa}{\sqrt{2\pi E}} = 0.00321 \tag{11b}$$

in which Young's modulus is taken to be 124.1 GPa (18,000 ksi). Substituting these quantities into Eqs. (7a-e), the parametric equations for the position of the match line on the da/dN (ΔK) plot are:

$$\Delta K = 1000 \sqrt{d_T} \tag{12a}$$

$$da/dN = 1.2\ m d_T = 0.012 d_T \tag{12b}$$

In the absence of inert atmosphere data, the $GRF_2(\Delta\varepsilon_{K2})$ curve is translated, match point on match line, as in Fig. 6b,c until it comes into the best correspondence, ΔK-wise, with the room air data. Then using the specific value of $\Delta\varepsilon_K$ from Eq. (11b), and the underlying value of the ΔK abscissa, as in Fig. 6, a value of d_T specific to this material can be calculated. From a rearrangement of Eqs. (7c,d),

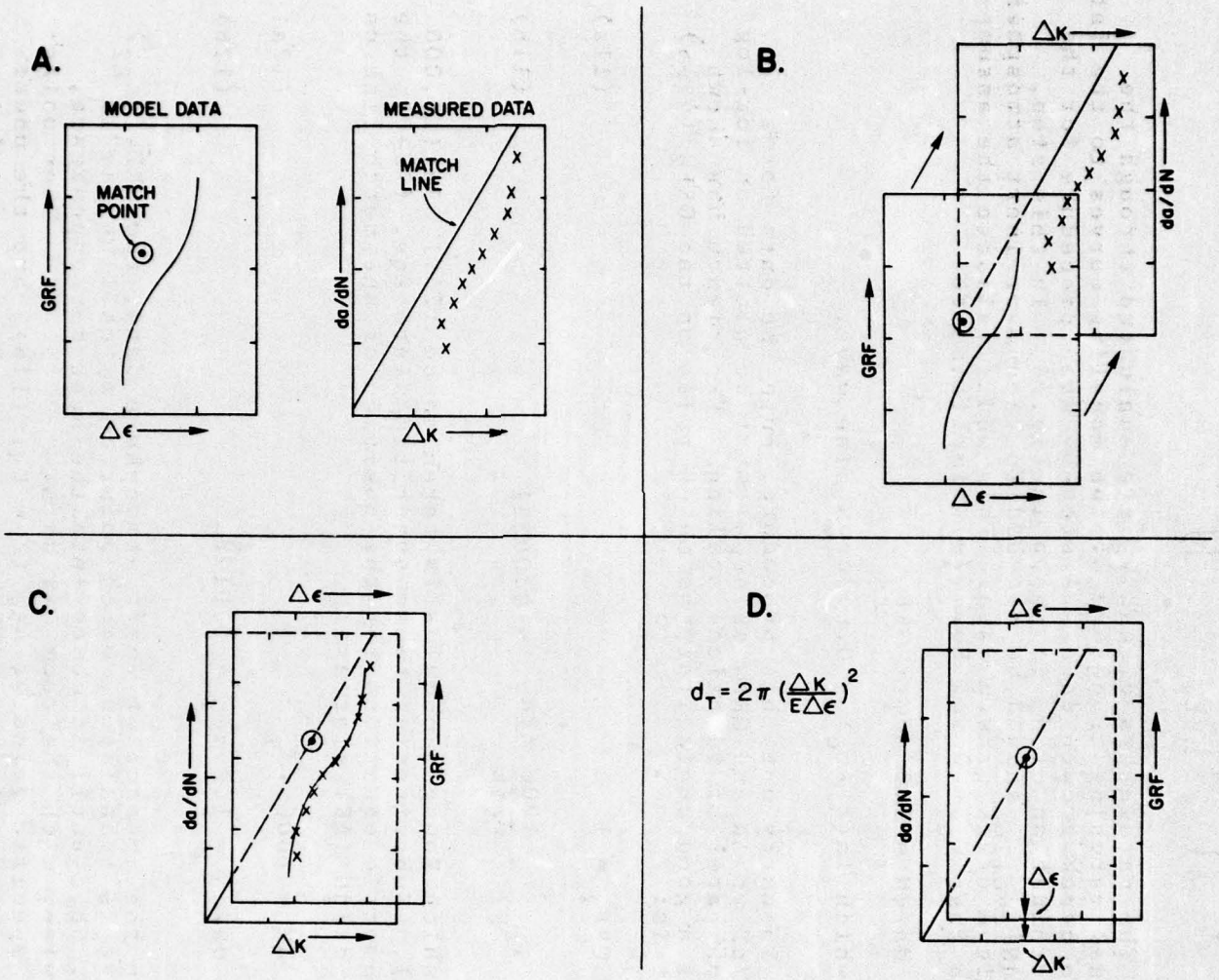

Fig. 6 — A schematic of the procedure for positioning the tensile ligament model predicted crack growth curves on the experimental data. The steps are described in the text.

$$d_T = 2\pi \left(\frac{\Delta K}{E \Delta \varepsilon_K} \right)^2 .$$

Since $\Delta\varepsilon_K$ was set equal to $1000/\sqrt{2\pi}$ E (in MPa), this simplifies to

$$d_T = \left[\Delta K \text{ (in MPa } \sqrt{\text{m}} \text{)} \right]^2 \qquad (13)$$

The curve is finally positioned by adding on the corrosion assistance contribution, Eq. 9c, with the V_s corresponding to the corrosion effects of room air and salt water, respectively.

The determination of V_s is achieved by trial, choosing values of $V_s \Delta t$, which, when substituted into

$$da/dN = 8Z\ V_s \Delta t \cdot GRF_1 + 1.2\ m d_T \cdot GRF_2$$

yield da/dN vs ΔK curves which "fair" through the data in the most satisfactory way possible.

PRESENTATION OF RESULTS

The resultant fatigue crack growth rate data is shown in Fig. 7. The data shows an amount of scatter which is typically expected of tests from different specimens. The modeling curves were applied in the manner prescribed in the previous section. As expected in the initial positioning, the $GRF_2(\Delta\varepsilon_{K2})$ modeling curve is located slightly under the room air data, as shown in the figure.

The match point overlays a value of $\Delta K = 2.95$ MPa $\sqrt{\text{m}}$. From this location, the computed value of d_T, from Eq. (13), is

$$d_T = (2.95)^2 = 8.7\ \mu\text{m}.$$

The predicted threshold for R = 0.1 is slightly below the lowest value of stress intensity at which data was recorded. Careful threshold level measurements would require lower loads and longer experimental times than could be allowed in the present effort. This may account for the difference between the measured and predicted threshold levels.

The lower frequency salt-water data commences at about the same applied stress intensity as the room air data, but shows the typical quick rise to a "plateau" level of essentially stress intensity independent growth rate before

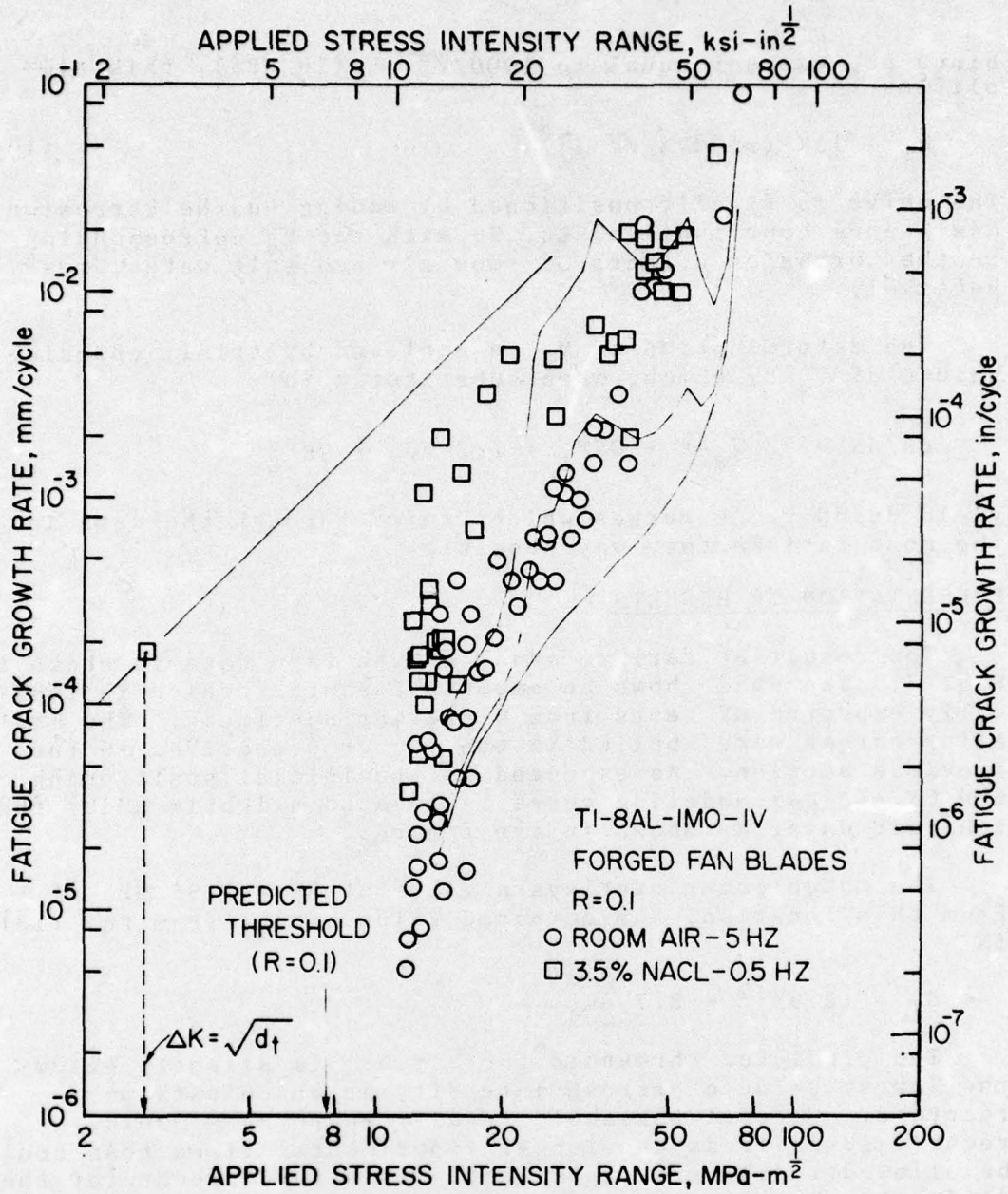

Fig. 7 -- The fatigue crack growth data from the forged fan blades, R = 0.1, both room air and salt water

merging again with the room air data in the region of stage III fatigue crack growth, i.e., that range of generally high growth rates exhibited by a crack approaching critical size. It is customarily argued that the plateau is due to the dominance of the mechanical component of fatigue crack growth by a stress-corrosion mechanism. As shown by Sullivan, the stress corrosion cracking plots for Ti-8-1-1 show a quick rise to a K-independent level in this case with a rate of about 0.4 mm/sec.

For relatively immune materials, such as Ti-6Al-2Nb-1Ta-0.8Mo [14], the corrosion assistance coefficient ($8ZV_s\Delta t$) is incorporated in the GRF_2 factor. However, for the very susceptible materials, such as this one, the corrosion term is incorporated as a factor for GRF, making the fatigue crack growth expression

$$da/dN = 8ZV_s\Delta t \cdot GRF_1 + 1.2md_T \cdot GRF_2$$

The determination of V_s is achieved by trial, choosing values of $V_s\Delta t$ which, when substituted in the equation above, yield da/dN vs ΔK curves which "fair" through the data in the most satisfactory way possible. The particular values were found to be 5×10^{-6} and 5×10^{-5} mm/sec for room air and salt water respectively. The amount and type of data collected for this study does not indicate whether this order of magnitude difference in the $V_s\Delta t$ term is due to a change in V_s or is entirely due to the difference in hold times of the 5 Hz and 0.5 Hz periods. Tests in both environments, at different frequencies, would be required to provide substantive conclusions about the corrosion contribution to fatigue crack growth.

It is important to understand the relationship of this data, from production quality fan blades which have seen in-service use, with the literature data developed from rolled plate furnished by the producer to the laboratories involved. Fig. 8 shows Bucci and Paris' data [4] on plate about 6.6 mm (0.26-0.27 in.) thick. Of the several frequency-environment-waveform conditions tested by these investigators, only the two which are most comparable to the present data are shown. The present data is represented by the modeling curve, which has the same position in this figure as in Fig. 7. It is seen that the data taken in dry argon lies slightly below, but has the same shape as the data from the fan blades. This is probably due not only to the inert environment of Bucci and Paris, but also to material differences. On the other hand, their salt water environment data exhibits a lower threshold than found for the fan blade material, but the rates eventually come up to about the same plateau level as in Fig. 7.

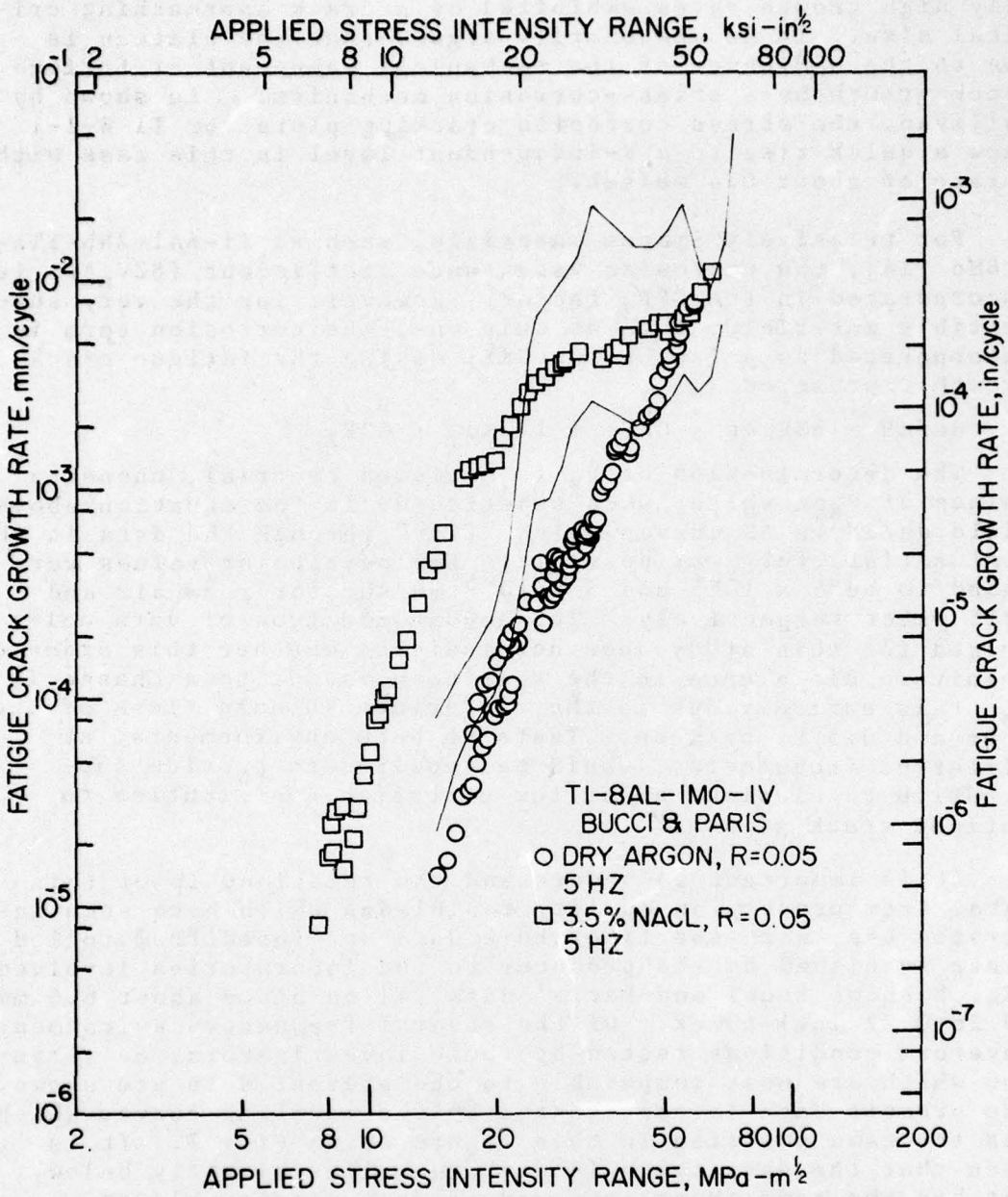

Fig. 8 — Fatigue crack growth data from Bucci and Paris (4). The curves are transposed from Fig. 7 to provide a means of comparison.

The higher frequency of the Bucci and Paris tests probably contributes to the difference in the approach of the salt water crack growth rates to the plateau.

Lastly the data of Meyn [3] is shown in Fig. 9. In general, this data shows the lowest growth rates, for a given set of conditions, than either the present work, or Ref. 4. The room air data of Meyn shows quite good agreement with that of Bucci and Paris. The vacuum data shows rates which are considerably slower, and essentially without the stage I-II-III structure which is usually expected over so large a range of rates. The 3.5% NaCl data, in spite of 0.5 Hz frequency, shows considerably slower rates for lower ΔK than either comparable study, but proceeds to higher rates for the larger ΔK levels.

DISCUSSION

During operation, the forces applied to the turbine blade are composed mainly of a large, essentially constant centrifugal force plus a vibratory dither due to slight blade imbalance and small allowable clearances in the engine's moving parts. However, the data of this study was acquired with a stress ratio of 0.1, as is customary, while the predominant load scheme applied to the blade involves larger ratios, close to unity. While this higher mean stress results in only small differences in crack growth rates as a function of the stress intensity range, there does appear to be an R-effect on the value of the fatigue threshold, which is the smallest value of applied stress intensity at which a fatigue crack will observably grow. There is, unfortunately, no reliable threshold data for Ti-8-1-1 to be found in the open literature. (Data in Ref. 4 on load ratio effects shows crack growth rates to only $\sim 10^{-5}$ mm/cycle, far from the accepted threshold-level rates of 10^{-7} - 10^{-8} mm/cycle). However, there is enough data available for Ti-6Al-4V to illustrate the effects of stress ratios on fatigue thresholds. Data from several sources [4,5,15] is shown in Fig. 10. This is not exactly threshold data in the sense that it is the value of stress intensity at which a crack will self-arrest, but rather it is a plot of the values of stress intensity at which the crack growth rates are some specific, small rate, as indicated. The point to be made is that the growth thresholds decrease, toward some small, but non-zero, value as the stress ratio increases.

---

15. R. P. Wei and G. M. Simmons, "Environment Enhanced Fatigue Crack Growth in High-Strength Steels," Proc. Int'l Conf. on SCC and Hydrogen Embrittlement of Iron-Base Alloys, Unieux-Firminy, France, 12-16 June, 1973.

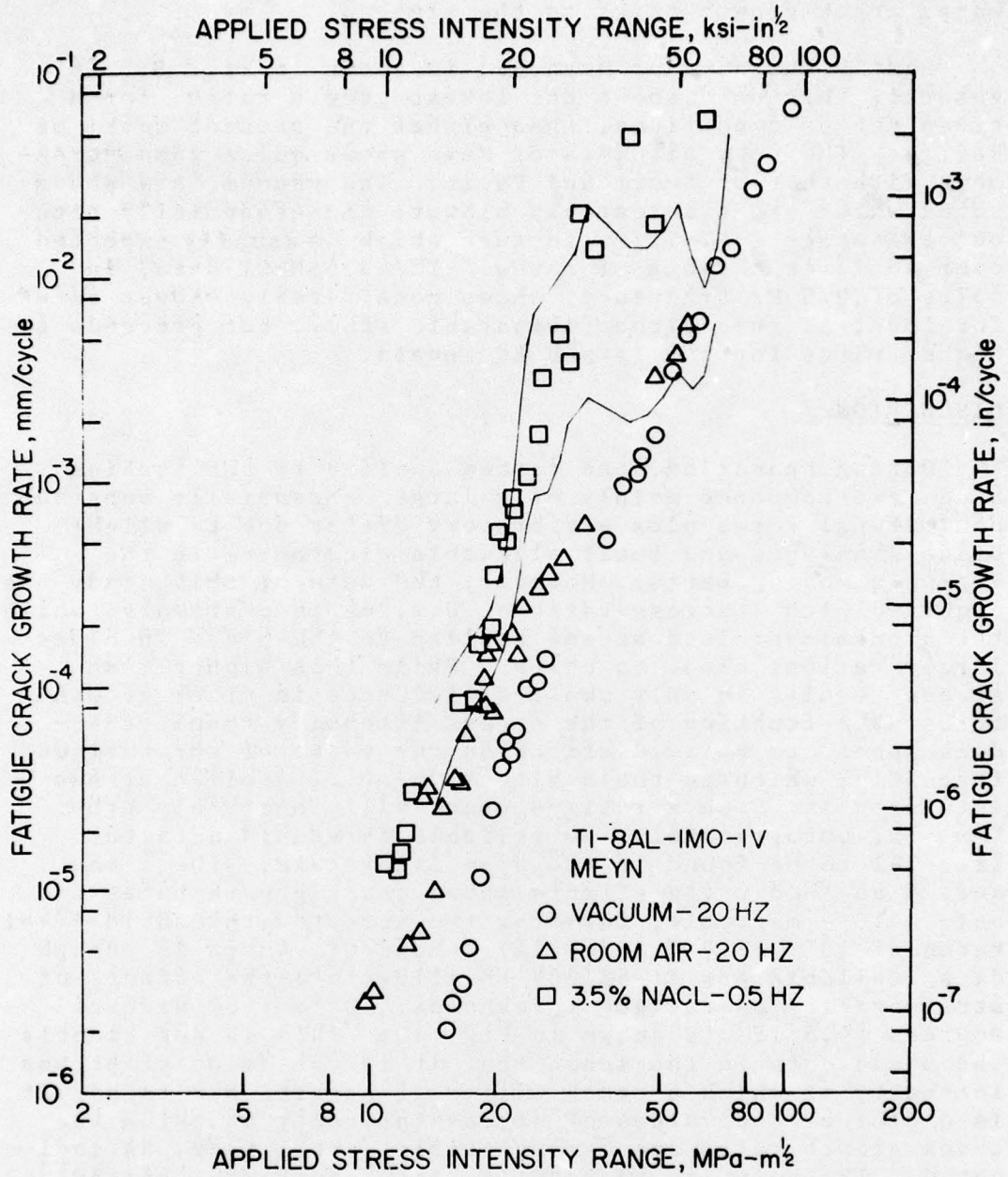

Fig. 9 — Fatigue crack growth data from Meyn (3). Again, the curves are transposed from Fig. 7.

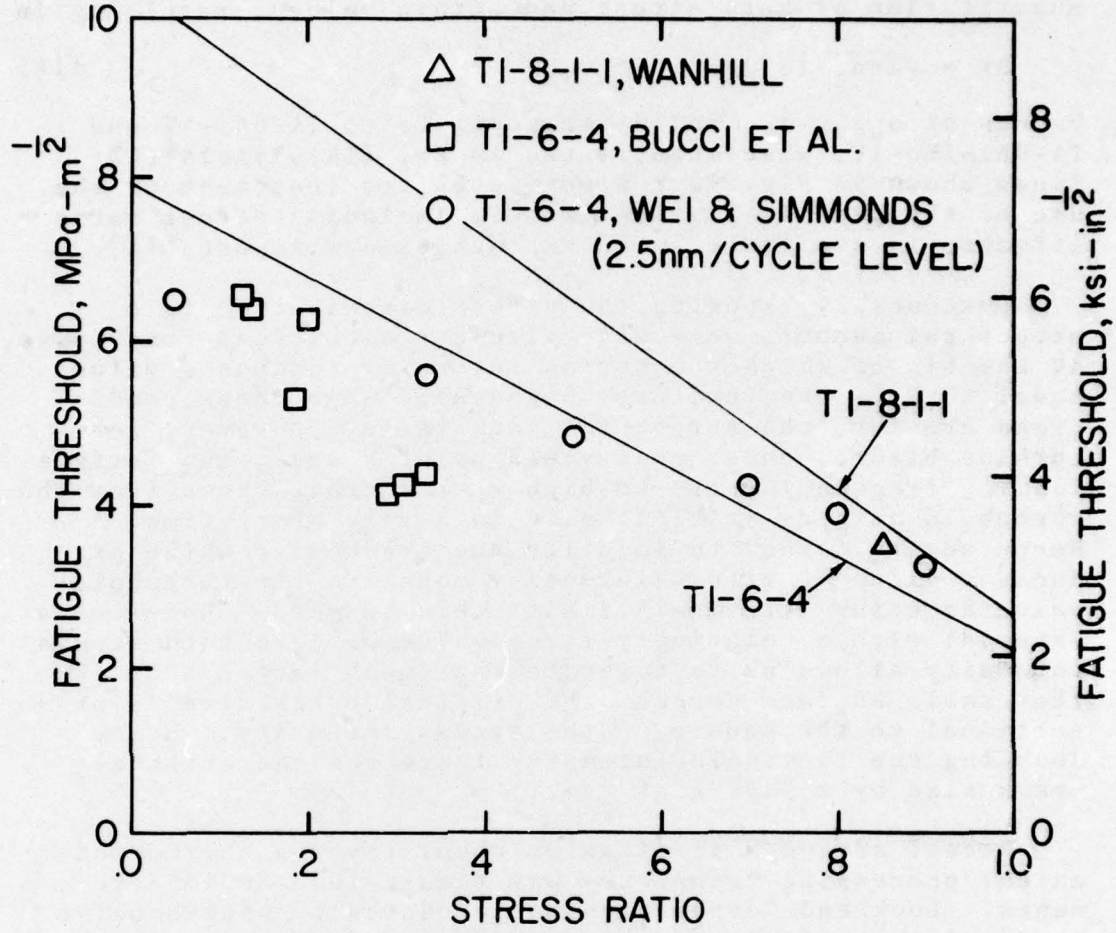

Fig. 10 — Threshold, or near-threshold stress intensity range values as a function of stress ratio. Most available work has been done for Ti-6Al-4V, but the decrease in threshold with increase in stress ratio is a general fact. The lines are the ligament model predictions of the fatigue threshold.

This has been shown to be true for other materials as well [16]. The tensile ligament instability model features a capability for the prediction of threshold values. Employing Eqs. (7a-d) for ΔK, the threshold is computed by substitution of zero stress and strain values, resulting in

$$\Delta K = \sqrt{2\pi d_T}\,(\sigma_{ucs} - R \cdot \sigma_{ys}). \qquad (14)$$

Values of σ_{ucs}, σ_{ys} and d_T appropriate to Ti-6Al-4V and Ti-8Al-1Mo-1V, when substituted in Eq. (14), yield the lines shown in Fig. 10. A more complete treatment of the use of the tensile ligament model, including stress ratio effects, is available as an NRL Memorandum Report [11].

Customarily, knowing the stress distribution in a structural member, we would calculate a critical crack size, at the tip of which the stress intensity reaches a value equal to K_{Ic}, the fracture toughness. When these conditions are met, the structural part fails. However, for turbine blades, under near yield point stress, the fatigue loading frequencies are so high that a crack grows from the threshold size to critical size in a very short time. Hence we are forced to identify the crack size which produces a value of stress intensity equal to the threshold value as being "critical". With this in mind, choice of a material with a relatively large value of threshold stress intensity allows us to tolerate that much larger a crack. (For small surface cracks, the critical crack size is proportional to the square of the stress intensity. Hence doubling the threshold intensity increases the critical crack size by a factor of four.)

Recent advances in titanium chemistry and thermomechanical processing techniques may result in some improvements. Lockheed Corporation has produced a comprehensive study of the effects of microstructures (resulting from processing variations) on the fracture properties of Ti-6Al-4V. The addition of rare earths to titanium-aluminum alloys has been shown to favorably affect ductility and

16. P. C. Paris, R. J. Bucci, E. T. Wessel, W. G. Clark, and T. R. Mager, "An Extensive Study on Low Fatigue Crack Growth Rates in A533 and A508 Steels," Scientific Paper 71-1E7-FMPWR-P7, Westinghouse Research Laboratories, Pittsburgh, Pennsylvania 15235, 1971.

creep resistance, two factors which affect fatigue performance [17, 18]. However, to the authors' knowledge, the direct measurement of the effect of rare earth additions on fatigue crack growth mechanics has not been carried out.

CONCLUSIONS

1. This work demonstrates the successful evaluation of the strain energy release rate ($\mathcal{J}$) via the crack opening displacement for titanium fan blades. The $\mathcal{J}$-value was used to compute stress intensity factors for partially cracked fan blades.

2. The crack growth rates in either air or salt water are nearly the same for the forged fan blade material as for conventionally rolled plate of the same Ti-8Al-1Mo-1V chemistry.

3. The tensile ligament model appears to adequately describe the thresholds for fatigue crack growth and the crack growth rates. The process zone size computed (8.7 μm) compares with that derived for other titanium alloys of approximately the same yield strength.

ACKNOWLEDGEMENTS

The authors would like to thank M. F. Blackburn of Pratt and Whitney Aircraft for information on the thermomechanical processing of forged titanium blades, and to J. M. Krafft, Mechanics of Materials Branch Head, for his advice and encouragement during the course of this research.

17. B. B. Rath et al., "Recrystallization and Grain Growth in Titanium Alloys," in The Effects of the Rare Earths on the Properties of Metals and Alloys, Proc. 1975 Materials Science Symposium, to be published in 1976.

18. G. S. Hall, "Effects of Yttrium on Microstructure of Titanium Alloys," in the Effects of the Rare Earths on the Properties of Metals and Alloys, Proc. 1975 Materials Science Symposium, to be published in 1976.